

Received November 19, 2017, accepted December 29, 2017, date of publication January 23, 2018,  
date of current version February 28, 2018.

Digital Object Identifier 10.1109/ACCESS.2018.2794463

# Impact of ICA-Based Image Enhancement Technique on Retinal Blood Vessels Segmentation

**TOUFIQUE AHMED SOOMRO<sup>ID</sup><sup>1</sup>, TARIQ MAHMOOD KHAN<sup>ID</sup><sup>2</sup>, MOHAMMAD A. U. KHAN<sup>3</sup>, JUNBIN GAO<sup>4</sup>, MANORANJAN PAUL<sup>1</sup>, AND LIHONG ZHENG<sup>1</sup>**

<sup>1</sup>School of Computing and Mathematics, Charles Sturt University, Bathurst, NSW 2795 , Australia

<sup>2</sup>Electrical Engineering Department, COMSATS Institute of Information Technology, Islamabad 45550, Pakistan

<sup>3</sup>College of Engineering and Computing, Al Ghurair University, Dubai 37374, United Arab Emirates

<sup>4</sup>The University of Sydney Business School, The University of Sydney, Camperdown, NSW 2006, Australia

Corresponding author: Toufique A. Soomro (tsoomro@csu.edu.au)

**ABSTRACT** An automatic retinal vessel segmentation method is proposed for quick and accurate segmentation of eye vessels. Such a method would play a vital role in analyzing many eye diseases. A retinal fundus image contains varying low contrasts, which undermine the performance of the segmentation process. Independent component analysis (ICA) is largely used for noise removal and consists of two architectures, designated as ICA1 and ICA2. We have validated both ICA architectures on retinal color fundus images and selected the one that provides improved contrast values. For retinal fundus, ICA2 architecture performed better than ICA1 by virtue of being more effective in compensating the low contrast values. Experiments conducted here validated the improvements over previously reported state-of-the-art methods. The impact of proposed segmentation model was assessed on publicly available databases like DRIVE and STARE. In case of the DRIVE database, the sensitivity increased 3% by (from 72% to 75%) while maintaining a segmentation accuracy of around 96%.

**INDEX TERMS** Retinal, segmentation, morphological filtering, ICA vessel enhancement.

## I. INTRODUCTION

Diabetic retinopathy (DR), glaucoma and age-related macular degeneration are common eye diseases that affect a blood vessel in light-sensitive tissue called the retina. Among them, the progression of Diabetic retinopathy (DR) is the most life-threatening as it results in definitive vision loss due to high sugar level and hypertension [1], [2] in later stages. It has been estimated that approximately 20 to 25 million people worldwide are affected [3], [4]. It is one of the leading cause of blindness and major vision loss in Australia, with approximately 1 in 7 Australians over 50 having some evidence of macular degeneration [4]. These diseases can lead to serious complications and even vision impairment or vision loss if it remains untreated [5], [6]. Early and accessible detection of ophthalmological diseases is especially important to prevent eye diseases from getting severe. It has been reported that about 95% of blindness can be prevented through early detection, timely treatment, and appropriate follow-ups procedure. For this reason, retinal image analysis is one of the modern methods for diagnosis of those progressive diseases [5].

Traditional ophthalmologists have used the fundscope for digital fundus photography, which is comprised of compound

optical system [7]. A fundus camera uses lenses to magnify views of the inner part of the retina. This inner part contains the optical disc, macula, and posterior poles [8]. Fundus camera operates in two modes, namely the fundus fluorescein angiogram mode and digital color fundus image mode. Fundus fluorescein angiogram mode is based on injecting fluorescein into a patient's nerves. Where fluorescein is a liquid that provided better visibility under ultra-violet light. When the light travels through vessels, its paths are illuminated and thus making it easier to inspect the blood flow in the retinal vasculature and subsequently provides a high-contrast image. Later, the image is evaluated through manual segmentation of vessels by an expert ophthalmologist [9], [10]. The method is time-consuming, making it difficult for a proper expert analysis to be quickly conducted, and can introduce significant delay. Digital color fundus image mode is based on automated segmentation and has the potential to reduce workload and increase the cost-effectiveness of eye screening [11]. Accurate vessel segmentation is a challenging task for researchers. The most popular existing methods are explained in the (section II) of this article.

The aim of this study is to observe the effect of the proposed contrast-normalization method on the extraction of retinal blood vessels. The study of retinal fundus images is a challenging task as it suffers from low and varying contrast, uneven brightness, and above all the uneven intensity of vessels itself. This can be linked with the very process of the diffusion rate of fluorescein, while the short has been taken. The influence of varying low-contrast and noise can be mitigated by using a suitable contrast-enhancement method such as independent component analysis (ICA).

The issues of varying low contrast as well as uneven illumination are addressed by first enhancing contrast in RGB domain and then converting RGB to greyscale. The process is explained in detail in the section IV of this paper. In the proposed technique, the first step is to eliminate the background noise and uneven illumination by using morphological operations. The second step is to enhance the visibility of tiny vessels by suppressing noise. For this task, we adopted a well-known algorithm FAST ICA (FAST Independent Component Analysis) [12]. Recently, ICA is gaining popularity by proving its success in diverse areas like image segmentation, face recognition, digital image forgery detection and medical images. We used ICA to enhance the retinal blood vessels against their background by suppressing noise in three independent components (RGB) of the color fundus image. ICA has two architectures that are used in the signal processing applications, in this paper, the performance of both architectures is observed for contrast normalization. This helps to select the suitable ICA architecture for the retinal fundus image. This paper presents three main contributions explained in details as follow.

- 1) A retinal image is typically made of three different pigments due to melanin, hemoglobin and macular, resembling with the three color channels of the retinal image. ICA can be used to determine three color channels as three enhanced independent components channels with potentially noise free contents.
- 2) There are two ICA architectures (ICA1 and ICA2), and it is important to select the more suitable for retinal fundus images. We have applied both architectures in the context of extracting noise-free independent components. Based on a contrast comparison of both architectures, we found ICA2 performing better than ICA1.
- 3) To implement proposed image enhancement technique, we employed a three-step process based on ICA2. The first step is to solve the noise issue, and the second step is to use ICA2 to enhance visualization of retinal blood vessels while the third step is to convert color RGB independent components into a single grayscale image.

After implementing contrast enhancement method, we study its impact on the segmentation of retinal blood vessels. For the post-processing stage, we used various proven enhancement schemes for vessels. More specifically, a multi-scale Laplacian-of-Gaussian detector, proposed by [13], is used here to enhance blood vessels. Finally, a binary conversion

based on a morphological flood-filled reconstruction method is employed for vessel segmentation.

The paper is organized as follows. Section II deals with related work. Section III explains the importance of ICA, its use and the effect of different types of ICA on retinal color fundus images. Section IV discusses the proposed methods. Section V discusses the post-processing steps. Section VI elaborates the composed algorithm of retinal vessel segmentation. Section VII discusses the databases and measuring parameters. Section VIII reports the experimental results. Finally, the conclusion and discussion are presented in Section IX.

## II. RELATED WORKS

In retinal images, the distribution of blood vessels is multi-directional and therefore difficult to isolate visually. Numerous enhancement filters (i.e Kernels) have been implemented in the past to enhance the visibility of blood vessels to obtain accurate segmentation [14], [15]. Recently, Lathen *et al.* [16] introduced the local-phase-based enhanced filter. It works as an intensity-based filter [14] to extract retinal blood vessels in the same vein.

Many other vessel-segmentation methods have been proposed in recent years [3], [17]. These methods can be divided into two types: supervised and unsupervised segmentation methods [18]. Supervised segmentation methods use pre-labelled samples to train a classifier such as the k-nearest neighbours classifier [19], support-vector machine (SVM) [20], [21], artificial neural networks (ANN) [22], and Gaussian mixture models (GMM) [11], [23]. Then the trained classifier is used to differentiate between the vessel and non-vessel pixels. Supervised methods require manually marked ground truth images in a database may need to extract the vessel and non-vessel pixels. On the contrary, unsupervised methods are based on imaging techniques to classify vessel and non-vessel pixels without training data or manually intervention. No requirement for training data makes the unsupervised method a more popular choice for vessel segmentation such as [15], [18], and [24]. Our proposed method in this paper comes under the unsupervised category.

There are different types of unsupervised segmentation methods, based on the thresholding technique [15], a combination of morphological path opening followed by thresholding, fusion [25] and active contour methods [18]. Obtaining the optimal thresholding with the threshold methods is very difficult. The problem with an active contour model is to formulate and optimize it according to image properties. Due to the manual iteration need, this process is time-consuming and often reaches local optima rather than global one. In this paper, an image-enhancement method and a contrast-sensitive approach are proposed to get a better-segmented image.

## III. INDEPENDENT COMPONENT ANALYSIS

The independent component analysis (ICA) is a statistical computation method for linear transformation of signals and

images that separate the statistically dependent mixture of signals or images into its components. Each component is statistically linearly independent of each other. The ICA can be elaborated in a better way from its mixed model as shown in Equation 1.

$$X = AS. \quad (1)$$

Equation 1 represents the ICA statistical model representing independent components. It is considered that the mixture vector  $X$  and independent component vector  $S$  are random vectors with zero mean (centered) and unit variance. The vector  $A$  is known as matrix  $A$  of the independent component. Matrix  $A$  is an unknown square matrix. It is also assumed that the independent component vector  $S$  has a non-Gaussian distribution. In ICA statistical models, the independent components have a non-Gaussian distribution. The main advantage of the ICA model is its ability to detect instances of a non-Gaussianity. The whole analysis is based on the random vector  $X$ . The main objective is to estimate the unknown components  $A$  and  $S$  using  $X$ . If the estimation of unknown mixing matrix  $A$  is possible then it is easy to compute its inverse as  $W$  and obtain the independent component vector  $S$ , given by:

$$S = A^{-1}X = WX. \quad (2)$$

$W$  can be estimated by using the FASTICA algorithm [12] which is based on initializing the random vectors. FASTICA is a well-known algorithm that is based on a fixed point algorithm giving one independent component. For multiple independent components, the FASTICA must run in the iteration  $n$  with components weight vectors  $w_1, w_2, w_3 \dots w_n$ . There is typically high probability of correlation between each vector values of the distinct component. To avoid the different random vectors converging at the same maxima, it is important to de-correlate or orthogonalizes the outputs of weight vectors  $w_1^T X, w_2^T X, w_3^T X \dots w_n^T X$  after each iteration. This orthogonalization can be done using the Gram-Schmidt-Orthogonalization method [26]. The ICA possesses two architectures for finding feature vectors. These two ICA architectures are used to determine the components of retinal images and observe the effectiveness of ICA on enhancing the contrast. These two ICA architectures (ICA1 and ICA2) are explained below in more detail as follows.

#### A. ICA ARCHITECTURE 1 (ICA1)

In ICA1, the image database is formatted as a matrix where each row represents an individual image. The ICA1 model is depicted in Fig. 1. In the ICA1 model, images are considered as random variables and pixels are deemed to be trials (i.e random process). From Fig. 1, a data matrix  $X$  (known as the mixture matrix) is the combination of  $n$  independent ICA components or images.  $W$  is known as the coefficient matrix, and it is calculated by using the FASTICA algorithm, where  $W$  should be a square pattern, and  $S$  is the source matrix of  $n$  independent basis images.

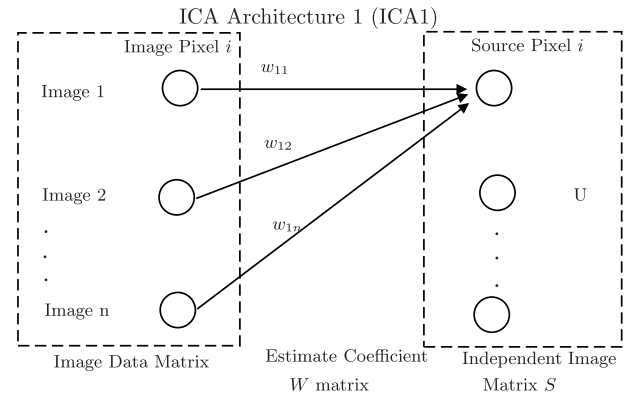


**FIGURE 1. ICA architecture 1 model.**

In ICA1, assume  $n$  training samples (with image column vectors of length  $m$ ) to represent the dimension of  $m \times n$  with column data matrix  $X = x_1, x_2, \dots, x_n$ . The main concept behind the implementation of ICA1 is the transposing of data matrix  $X$ , such as  $Y = X^T$  as a mixture row data matrix. The  $Y$  is represented as  $Y = y_1, y_2, \dots, y_m$ . The following steps are adopted to implement ICA1.

#### 1) CENTERING PROCESS

In the first step, the mean vector is estimated from the data matrix as  $\mu_I = \frac{1}{m} \sum_{j=1}^m y_j$ . This representation of the mean vector depends on subtracting from each column vector of the data matrix such as  $(y_j - \mu_I) \rightarrow \bar{y}_j \rightarrow \bar{y}_v \cdot \bar{y}_v$  represent the vertically centered row data matrix. The mean vector is subtracted from each column vector. This generates zero mean image row data matrix.

#### 2) WHITENING PROCESS

The next task entails whitening the centered data matrix by using the principal component analysis (PCA) technique. It can be performed by orthonormal eigenvectors  $V = v_1, v_2, v_3 \dots v_n$  of the covariance matrix  $\sum_I = \frac{1}{m} \sum_{j=1}^m y_j y_j^T$  according to the data matrix that considers the largest positive eigenvalues ( $p$ ) as  $y_1 \geq y_2 \geq \dots \geq y_p$ . Mathematically, the whitening can be expressed as:

$$H = V D^{-\frac{1}{2}}. \quad (3)$$

Where  $D$  is the diagonal matrix of the largest eigenvalues.

#### 3) TRANSFORMATION PROCESS

After whitening, the data matrix  $\bar{y}_v$  is transformed as:

$$\tilde{y} = H^T \bar{y}_v. \quad (4)$$

These three steps are very important for applying ICA, and they are referred to as the pre-processing steps of ICA. Once these steps are applied, ICA will be performed on the whitening data matrix  $H$  and achieve a matrix  $S_I$  consisting of random independent row-wise images, that is  $S_I = W_I \tilde{y}$ .

Where  $W_I$  is known as the coefficient matrix of ICA. The row vector of  $S_I$  corresponds to the base images of ICA1. The final independent images are achieved through the vertically centered data matrix projecting on the independent eigenvectors of base images as  $Z = \bar{y}_v S_I^T = \bar{y}_v \tilde{y}^T W_I$ .  $Z$  is an independent component of the image, and the number of independent images depends on the user's requirements. We apply this to each channel of a color retinal image so that we have three independent components in ICA1.

### B. ICA ARCHITECTURE 2 (ICA2)

The data matrix  $X$  is organized in the column vector, which is considered to be an image. The input image data matrix  $X$  is transposed from the ICA1 since ICA2 is an inversion of ICA1, i.e. in ICA2 the pixels are variables and the images are trials. The ICA2 model is shown in Fig. 2.

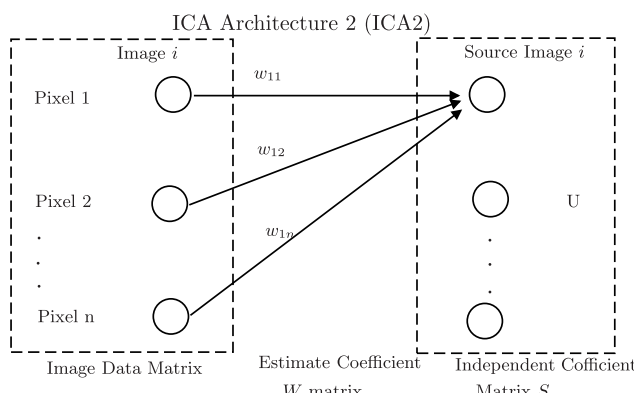


**FIGURE 2. ICA architecture 2 model.**

Consider data matrix  $X = x_1, x_2, \dots, x_n$  of dimension  $m \times n$ . The  $n$  training sample of length  $m$  of the data matrix is arranged column-wise. Similarly, ICA2 consists of two processing steps, namely centering and whitening. In the centering stage, mean vector  $\mu_H = \frac{1}{n} \sum_{j=1}^n x_j$  is subtracted from each column of the data matrix  $X$ . Mathematically, it is represented as  $(x_j - \mu_H) \rightarrow \bar{x}_j \rightarrow \bar{X}_h$ .  $\bar{X}_h$  is called as centered horizontal column of the data matrix. Subsequently, the mean vector is subtracted from each column according to the image resolution. Following the centering process, the  $\bar{X}_h$  becomes the zero mean image. The remaining stages in the ICA2 model resemble those of ICA1. The independent co-efficients are obtained in the form of column  $S_H = W_H H^T$ . The output independent images are obtained through a horizontally centered data matrix projected onto this independent coefficient matrix as  $Z = S_H \bar{X}_h$ .

### IV. PROPOSED METHOD

The ICA-based proposed image enhancement model is shown in Fig. 3. The image enhancement technique is based on three steps elaborated as follows.

### A. NON-UNIFORM BACKGROUND REMOVAL

An acquired fundus color image contains three channels: red, green and blue. All three channel images show considerable variation in background pixels intensity due to uneven illumination. The morphological operations are used to correct non-uniform illumination for each color channel of the retinal fundus image. The background of each color channel is estimated by using mathematical morphology. The estimated background is subtracted from the original image. The morphological operation sequence is named as a top hat of the image. The main purpose of top hat operation is to remove high frequencies (considered to be the reflectance of the image) and retains low frequencies (deemed an illumination of the image). The black top hat  $closing(f(x, y))$  is used for clear background and the white top hat  $mean(closing(f(x, y)))$  is utilized for the dark background. Since the background is clear in the retinal images, the corrected image  $g(x, y)$  is obtained using:

$$g(x, y) = [f(x, y) - closing(f(x, y))] + mean(closing(f(x, y)))$$

The structuring element chosen for the morphological closing operation is a disk with a radius of 11. The radius of the disk is selected to be slightly larger than the largest width of the vessels present in the database. The results of these steps are shown in Fig. 4) with percentage improving the uneven illumination. The process is adopted for all three channels independently so that the illumination issue is addressed.

To evaluate the performance of background correction, we adopted a procedure as follows. The corrected images are first adjusted same mean and standard deviation. The image is divided into  $10 \times 10$ . The uniformity metric is defined in terms of background standard deviation  $\sigma$  as.

$$\sigma = \sqrt{\frac{1}{N}(\mu_K - \mu_0)^2}. \quad (5)$$

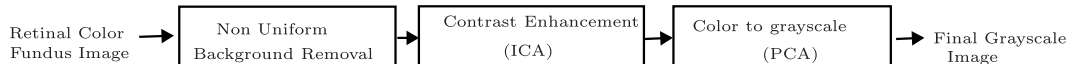
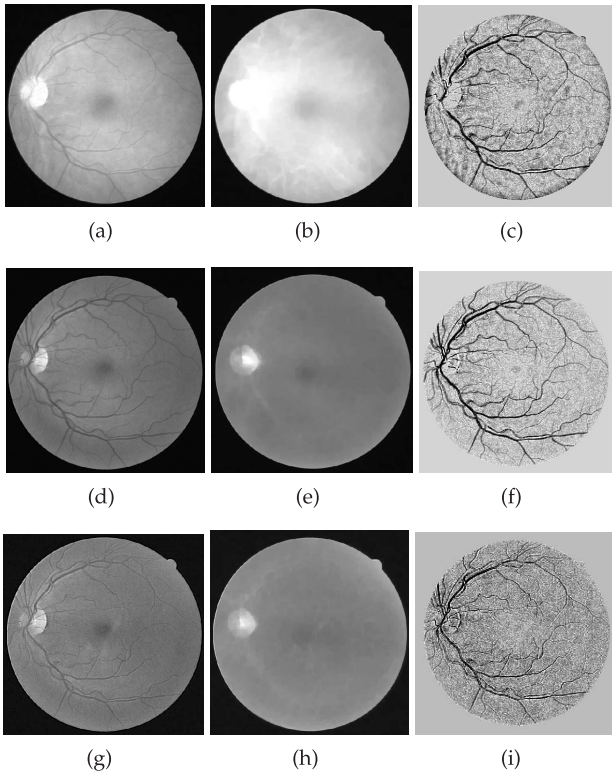
Where  $N$  is represents the number of pixels and  $\mu_K$  is mean pixel value of Kth sub image, and  $\mu_0$  is

$$\mu_0 = \frac{1}{N} \sum_k \mu_K. \quad (6)$$

A lower background standard deviation  $\sigma$  is related to the more uniform backgroud image, and it is expected that a successful non-uniform background removed images should be related with the reduction in value of  $\sigma_\mu$ .

We also measured the contrast of the retinal blood vessels of non-uniform background removal images by selecting 200 blood vessels and background intensity point. The pictorial illustration of computing contrast is shown in the Fig. 5.

Statistically, the contrast of the retinal blood vessels surrounding in contradiction of their background of the retinal image is explained as an absolute mean intensity difference between the retinal blood vessels intensity values and their background intensity values, and it is represented as

**FIGURE 3.** Proposed image enhancement model.

**FIGURE 4.** Non-uniform background removal step results for three retinal images: Fig (a) Red channel image with background standard deviation of 0.085 , Fig (c) corrected uneven illumination image with background standard deviation of 0.079 (6% reduction) and Contrast:48.15. Fig (d) Green channel image with background standard deviation of 0.087, Fig (f) corrected uneven illumination image with background standard deviation of 0.079 (8% reduction)and Contrast:51.98. Fig (g) Blue channel image with background standard deviation of 0.081, Fig (i) corrected uneven illumination image with background standard deviation of 0.073 (9% reduction) and Contrast:43.21.

in Equation 7.

$$C_{|bv-bg|} = \left| \frac{1}{n} \left( \sum_{i=1}^n I_{bvi} - \sum_{i=1}^n I_{bgi} \right) \right| \quad (7)$$

In Equation 7,  $I_{bvi}$  represents retinal blood vessels intensity values where as  $I_{bgi}$  represents retinal background intensity values.  $n$  represents number of pixels selected for retinal blood vessels and their background, as it is suggested  $n = 200$ , and these intensities values are selected randomly.

#### B. CONTRAST ENHANCEMENT USING ICA

Independent component analysis (ICA) is modeled on the output of each color channel of the fundus image from the non-uniform background output image. It is important that the imaging and biological properties of the image are well

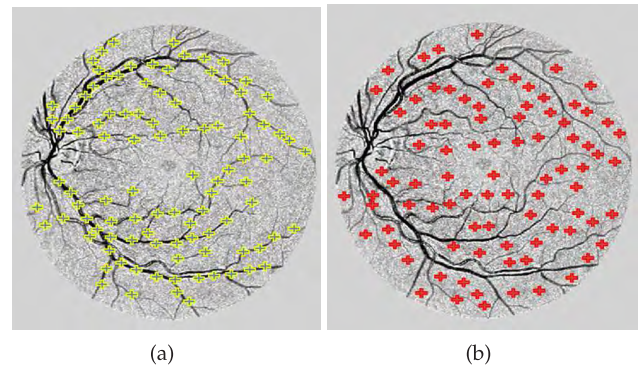


**FIGURE 5.** Selection of intensity data points (blood vessel (Blue points indicate blood vessel pixel selection) and background (Red points indicate background pixel selection)): (a) Blood vessels pixel selection of Image. (b) Background pixel selection of image.

understood before applying ICA for the purposes of enhancement. According to the retinas biological structure, it contains two main classes of eye structure, ocular media, and ocular fundus [27]. Cornea, lens and vitreous are the main components of the ocular media, placed between the viewer and the ocular fundus. Sclera, choroid, retina and retinal epithelium are the main elements of the ocular fundus. The retinal epithelium contains different pigments, and thus a more enhanced reflectance image can be achieved from these pigments [28]. The retinal pigments are macular, hemoglobin and melanin. Retinal pigments give us a good idea of how to modeling the retinal fundus, according to the similar properties shared by the retinal pigment and color fundus images. These include, for example, a retinal image containing the distribution of melanin, hemoglobin and macular pigment (similar color retinal fundus images contained red, green and blue channels). These three retinal pigments are linearly independent, and similarly, retinal color channels are also linearly independent. The red channel contains most of the luminance information as well as a lot of noise; the green channel has the least noise, and the blue channel has shadows as well as noise. In this study, we focus on determining a suitable retinal pigment from the output image of each channel of the fundus image that contains well-contrasted blood vessels. To do this, ICA is applied to each non-uniform background output image to increase the contrast level of the tiny blood vessels against their background.

We have applied two ICA architectures. The main objective is to observe which ICA architecture works better on the retinal images in terms of enhancing the contrast of retinal blood vessels. Fig. 6 shows the output images of ICA1 and ICA2 concerning each color channel of the retinal image. It is clearly observed that output images of ICA2 give a better

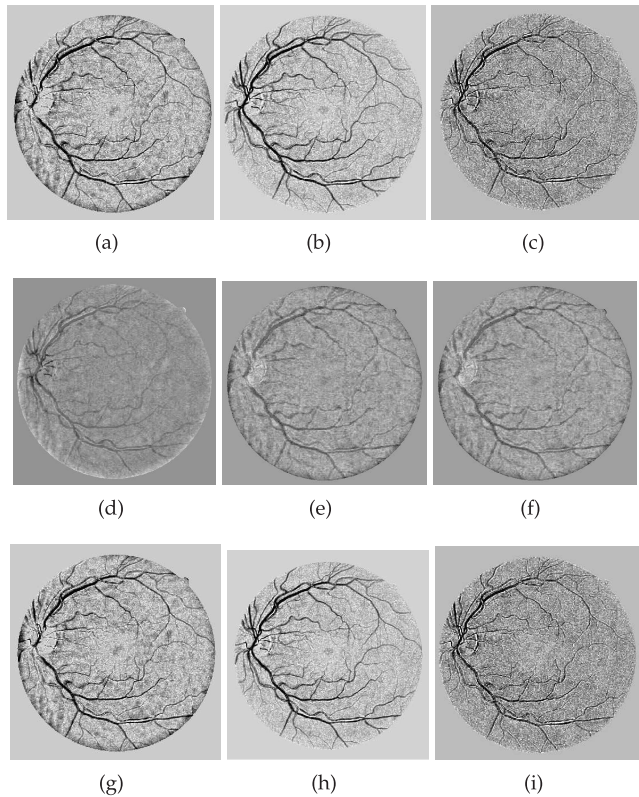


**FIGURE 6.** Proposed fundus image ICA architectures model results: Fig (a) Red corrected uneven illumination image (Contrast:48.15); Fig (b) Green corrected uneven illumination image (Contrast:51.98); Fig (c) Blue corrected uneven illumination image (Contrast:43.21); (d) Red component of ICA1 (Contrast:18.87); (e) Green component of ICA1 (Contrast:25.01); (f) Blue component of ICA1 (Contrast:24.97); (g) Red component of ICA2 (Contrast:51.02); (h) Green component of ICA2 (Contrast:59.15); and (i) Blue component of ICA2 (Contrast:47.54).

contrast of vessels against their background than ICA1 images. We measured the contrast of each channel of ICA1 and ICA2. There is around 30% contrast improvement achieved in ICA2 than ICA1 in each channel. For more validation, we compare the histogram of each channel of retinal fundus image resulted from ICA1 and ICA2. It is clearly observed from Fig 7 that the histograms of RGB components of ICA2 gives better spread and represents many more levels of than ICA1 images histograms. The ICA2 is performing much better on retinal images, and it gives better vessels segmentation as explained in the post-processing section.

Based on the analysis between ICA1 and ICA2, ICA2 gives a much better-enhanced image. For further validation, we compared the ICA2 enhanced images with other contrast enhancement methods on retinal images. These methods are retinex image enhancement technique, image local enhancement, homomorphic filtering and global inter-image enhancement. Figure 8 shows the comparison of these enhancement method output image with our proposed ICA2 enhanced image. It is clearly observed that ICA2 gives the better visualisation of retinal vessels as compared to other enhancement methods.

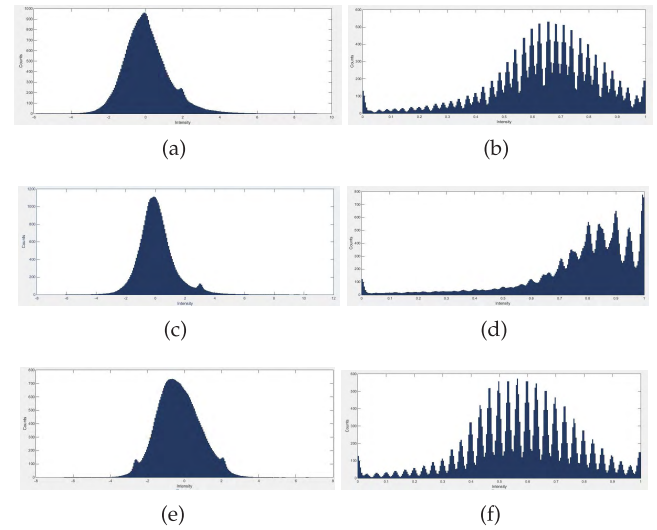


**FIGURE 7.** Observation based on a comparison of ICA1 and ICA2 of RGB components. Fig (a and b) represents the histogram of Red component of ICA1 and ICA2. Fig (c and d) represents the histogram of Green component of ICA1 and ICA2. Fig (e and f) represents the histogram of Blue component of ICA1 and ICA2. The analysis makes clear that the ICA2 images histogram contains well spread intensity profile with better equalization than ICA1 images.

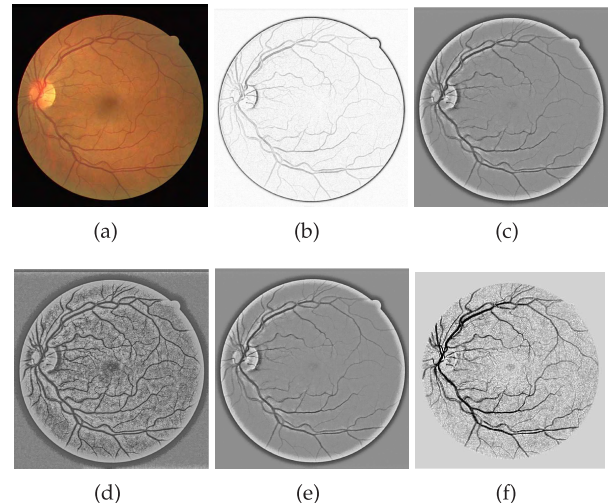


**FIGURE 8.** Comparison of enhancement techniques with ICA2 enhanced image. For illustration, we compared the green band image of ICA2 with green band of other image enhancement techniques. Fig (a) is color retinal image. Fig (b) is retinex enhanced image. Fig (c) is output of image local enhancement. Fig (d) is output of homomorphic filtering image. Fig (e) is output of global inter-image enhancement, and Fig (f) is proposed ICA2 enhanced image.

### C. COLOR TO GREY SCALE USING PCA

After adjusting the contrast of the image, the next essential task is to combine three color channels (red, green and blue) into a single channel grey scale image. This is required to reduce the amount of data to be processed through the segmentation stages. Many researchers have selected the green channel as the best contrast image [29]–[31]. We prefer choosing all three channels with the help of the principal component analysis (PCA) to achieve the well enhanced single grey scale image.

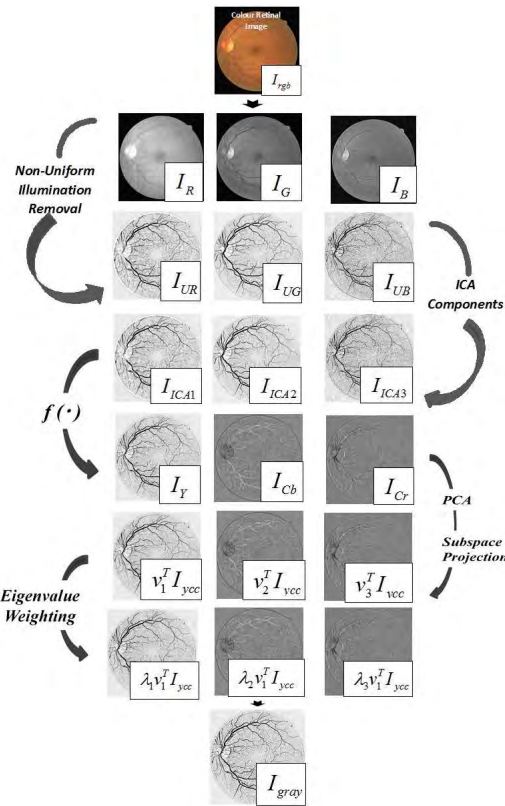


**FIGURE 9.** The PCA based color to grey retinal fundus image model.

The color-to-grey conversion is used to combine all three color channels that are already treated with their respective non-uniform removal and contrast enhancement processes. The first stage of the color-to-grey conversion method is a formation of vector color images ( $I_{rgb} \in R^3$ ) by stacking the three color channels side-by-side. Then, a YCbCr image ( $I_{YCbCr} \in R^3$ ) is computed from its RGB version to separate the luminance and chrominance channels using conventional transfer function  $f(\cdot)$  as defined in [32]. Next, the eigenvalues  $\lambda_1 \geq \lambda_2 \geq \lambda_3 \in R^1$  and their corresponding eigenvectors  $v_1 \geq v_2 \geq v_3 \in R^2$  are found by adopting the PCA method. The final grey image  $I_{gray}$  is calculated by a weighted linear combination that considers three main factors. These specifically are the length, width, and orientation of two filters, where weights are calculated by the percentage of their eigenvalues. The final output is scaled to  $[0, 1]$  as shown in Fig 9. The histogram of  $I_{gray}$  is shown in Fig 10(d), which is more spread and represents many more levels of intensity when compared to that of the ICA image histogram as depicted in Fig 10(b).

## V. POST-PROCESSING

Segmentation of retinal blood vessels is performed by using two steps, proposed by [33], with the proposed contrast-normalisation method being incorporated. These two steps are described in more detail as follows.

- 1) Coherence of Retinal Blood Vessels.
- 2) Binary Output

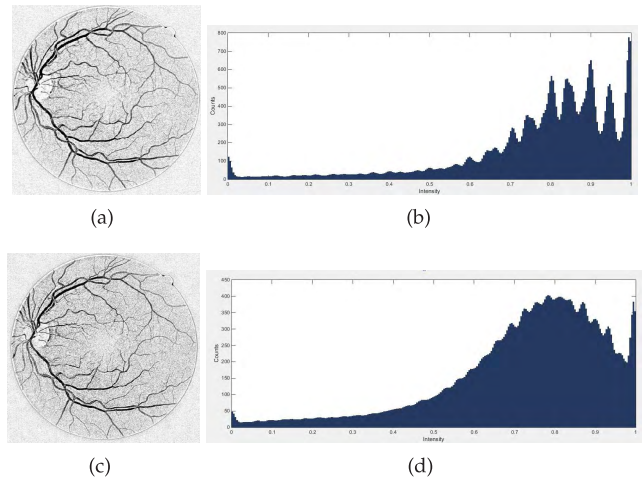


**FIGURE 10.** Contrast improvement observation based on a comparison of ICA green channel image and PCA grey scale image. Fig (a) shows the ICA2 green channel image (Contrast:59.15) along with its histogram (as Fig (b)). Fig (c) depicts the PCA-based grey image (Contrast:63.27) along with its histogram (as Fig (D)). It The analysis makes clear that the PCA grey image histogram contains well spread intensity profile with better equalization than ICA green channel image and provide better contrast ratio numbers.

## A. COHERENCE OF RETINAL BLOOD VESSELS

Although the proposed normalization improves the overall contrast of the retinal image, it is evident that discontinuities in the vessels exist and this problem needs to be addressed. For this reason, Second-order Multi-Scale Laplacian of Gaussian detector is used to fill the gaps of connecting vessels and provide the coherent region of vessels, as shown in Fig. 11. Even after filling the gaps, large vessels are illuminated with good contrast as compared to tiny capillaries because small vessels/capillaries do not maintain the same level of coherence against their background. This makes the binarization of the vessels in their current form difficult. To tackle this problem, an anisotropic oriented diffusion filtering, suggested by [34], is applied to boost the coherence of tiny vessels. The Second-order Multi-Scale Laplacian of Gaussian detector and an anisotropic oriented diffusion filtering technique are explained below.

### 1) SECOND-ORDER MULTI-SCALE LAPLACIAN OF GAUSSIAN DETECTOR

In retinal fundus images, vessels can be approximated with geometric shapes known as ridges. The simplest way to suppress noise and to detect ridge structure is to apply a second-order derivative oriented in a specific direction. The filter works on the three parameters, i.e. length  $\sigma_u$ , width  $\sigma_v$  and orientation. The length  $\sigma_u$  is tied to be multiple of width  $\sigma_v$  for maintaining the elongation. The width parameter  $\sigma_v$  is chosen from the set {4, 5}, and the validation process to select the best scale normalization parameters is elaborated in the results section VIII-B. The maximum responses among length, width and orientation are selected. A generalized

two-dimensional Gaussian function is used, given by:

$$g(u, v) = \frac{1}{2\pi\sigma_u\sigma_v} \exp\left(-\left(\frac{u^2}{2\sigma_u^2} + \frac{v^2}{2\sigma_v^2}\right)\right). \quad (8)$$

It poses two independent parameters  $\sigma_u$  and  $\sigma_v$ . Now taking its second-derivative with respect to  $u$  only gives:

$$g_{uu}(u, v) = \frac{1}{2\pi\sigma_u^5\sigma_v} \left(u^2 - \sigma_u^2\right) \exp\left(-\left(\frac{u^2}{2\sigma_u^2} + \frac{v^2}{2\sigma_v^2}\right)\right). \quad (9)$$

The discrete kernel is rotated in a specific orientation is  $u = x \cos \theta - y \sin \theta$  and  $v = x \sin \theta + y \cos \theta$ . The output response of the oriented kernel is normalized by multiplying it with a factor  $\sigma_u^\alpha \sigma_v^\beta$ . Optimal values for  $\alpha$  and  $\beta$  are calculated for ideal ridge patterns in [35], and the values are  $\alpha = 1.5$ , and  $\beta = 0.5$ . However, our focus here is to elevate the detector intensity of small-width vessels that have a lower contrast as well. To this end,  $\alpha = 1$  and  $\beta = 0.5$  seem more appropriate choices for our database images. Using these factors for scale-normalization, the maximum for each pixel is determined, and this means probing all different length, width and orientation combinations. The output of this process is shown in Fig. 11.

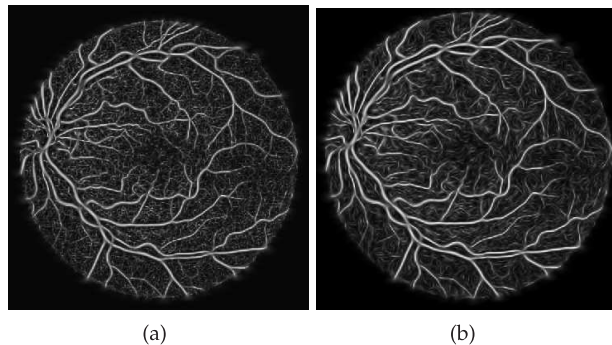


**FIGURE 11.** Second-order multi-scale gaussian derivative detectors outputs: (a) Initial output with maximum value; and (b) Initial output after normalised factor.

## 2) ANISOTROPIC ORIENTED DIFFUSION FILTER

To remove the noise and improve the appearance of small vessels, the anisotropic diffusion scheme presented in [36] is applied. The diffusion process consists of the following steps:

- 1) Calculate second-moment matrix for each pixel.
- 2) Construct diffusion matrix for each pixel.
- 3) Calculate the change in intensity for each pixel as  $\nabla(D\nabla f)$ .
- 4) Update image using difference equation as:

$$f^{t+1} = f^t + \Delta t \times \nabla(D\nabla f) \quad (10)$$

## B. BINARY OUTPUT

After conducting the diffusion binarization, some intensity differences still exist along with the length of the vessels. To achieve superior binary output, it is always better to implement the mix of some local strategies bounded by some global

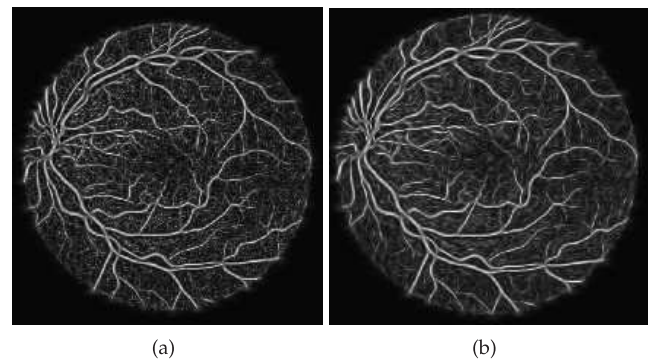


**FIGURE 12.** Oriented diffusion outputs: (a) Retinal image before coherence anisotropic diffusion filter; and (b) Coherence anisotropic diffusion filter.

threshold to extract the small blood vessel vasculature of the retinal fundus image. For this purpose, a region growing tactic with tactically located seed points is usually adopted, where a global threshold is employed to stop the region of spread. For example, a region-growing method was used in [37].

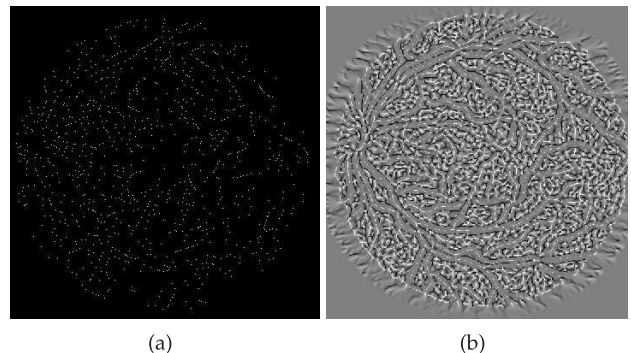


**FIGURE 13.** a) shows localized seed points. b) shows the response of isophote curvature detector.

Once the required vessel seed point from region growing method is achieved, as shown in Fig.13(a), the proposed flood-filled tactics can be utilized to produce the estimated accurate binary image [38]. To acquire the proper vessel binary image, flood-filled tactics, usually called morphological image reconstruction [38], can be used. It contains two types of input images: one is known as the marker, providing the seed points to be grown; and the second image is known as the mask image. The seed points from a marker image are dilated or spread out while being forced to fit in the mask image. This dilation process continues until the image values stop changing. In our research work, however, the marker image is the seed image and it is already available from the threshold of the isophote curvature output, as shown in Fig. 13(b). Subsequently the primary task of our study is to have a suitable mask image. We adopted the morphological process to obtain such a binary image. The result of the morphological image reconstruction process is shown in Fig.14. This process leads to an improved binary outcome without missing tiny vessels.

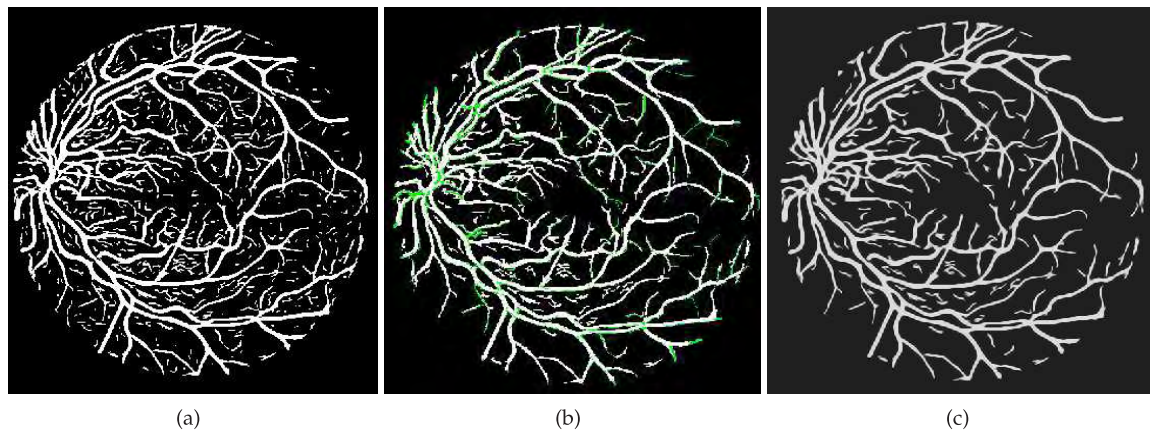


**FIGURE 14.** (a) Mask image; (b) Missing vessels image (shown with Green); and (c) Output image without missing vessels.

## VI. COMPOSED ALGORITHM

The procedure adopted for retinal vessels segmentation is outlined as follows:

- Stage 1:* The first stage handles the issue of uneven illumination. Morphological tactics are implemented to overcome uneven illumination from each channel of the retinal color fundus image.
- Stage 2:* Proposed ICA enhancement is applied to each channel output of the previous image to obtain well-contrasted images.
- Stage 3:* The third stage handles conversion of a color image into a grey image, while the PCA color-to-grey conversion method is implemented for retinal images to achieve a well-contrasted grey image.
- Stage 4:* This stage is concerned with boosting the vessels, which is based on the second-order detector scale normalization parameters named  $\alpha$  and  $\beta$ .
- Stage 5:* After scale normalization, the uneven intensity of vessels still exists along with some broken ridges. To tackle with this problem, anisotropic oriented diffusion filtering is used.
- Stage 6:* The flood-filled morphological reconstruction method is used to obtain a well-segmented vessels image.

## VII. DATABASE AND MEASURING PARAMETERS

### A. Databases

To validate our methodology, the two publicly accessible databases named Digital Retinal Images for Vessel Extraction (DRIVE) [19] and Structured Analysis of the Retina (STARE) [39] database are used. The DRIVE database contains 40 images of two pairs, testing and training images. These images have resolutions of  $768 \times 584$  pixels and contain masks and manual ground truth images. The STARE database contains 20 images, of which 10 contain different abnormalities of eye diseases. It, therefore, provides us with a good chance to validate our algorithm on such challenging images. These images have a resolution of  $605 \times 700$  pixels.

Their masks images, as well as ground truth images, are also available.

The advantage of using both databases is that they contain many segmentation images as ground truth and many researchers used these databases for validating the performance of a segmentation algorithm. It provides an opportunity to fairly compare the performance of proposed method with other existing methods.

### B. MEASURING PARAMETERS

There are three commonly used parameters to evaluate the performance of retinal blood vessels segmentation methods [40]. These parameters are accuracy, sensitivity, and specificity. Specificity and sensitivity impart information regarding true and false vessels and non-vessels pixels detection, whereas accuracy gives information on the overall segmentation of vessels pixels. The main purpose of this work is to improve the detection of vessels and non-vessels pixels, which can be achieved by increasing the sensitivity of the method.

## VIII. EXPERIMENTS AND RESULTS

This section is organized into five subsections. The first subsection explains the effect of the performance of segmentation methods with ICA and without ICA. The second subsection elaborates the effect of firstly, scale normalization parameters on the segmentation model; and secondly, suitable scale normalization parameters. The third subsection explains the effect of stopping time of anisotropic diffusion filters on the segmentation model. The performance of our proposed method on challenging retinal color fundus images is covered in the fourth subsection. The fifth and last subsection compared our method with other existing methods.

### A. ANALYSIS ON THE EFFECT OF ICA

To test the effectiveness of the proposed method, the performance of segmentation model is accessed with and without ICA. The segmentation model with ICA is exactly the same

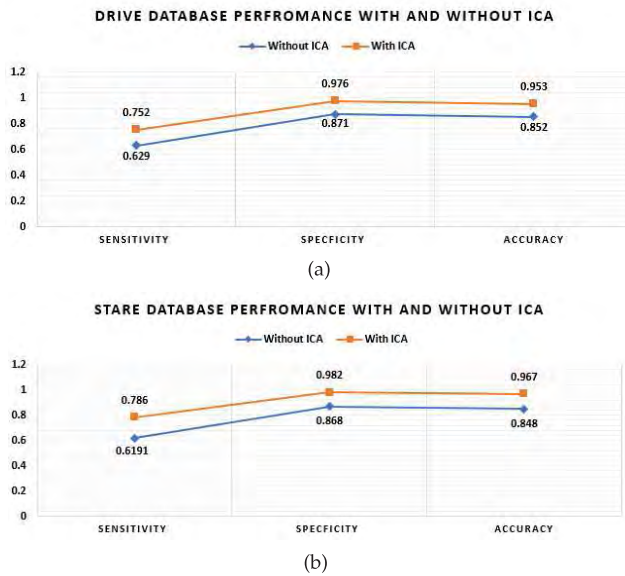


**FIGURE 15.** Performance analysis of segmentation method with ICA or without ICA.

as that explained in the composed algorithm section. The segmentation model without ICA means the same steps as used in the composed algorithm except ICA stage 3. It is observed that sensitivity of the proposed method is 0.752 and 0.786 on DRIVE and STARE databases respectively. Without ICA, it gives lower sensitivity on both databases, that is 0.629 and 0.619 on DRIVE and STARE respectively. Similarly, It is observed that accuracy of the proposed method is 0.953 and 0.967 on DRIVE and STARE databases respectively. Without ICA, it gives lower accuracy on both databases, that is 0.852 and 0.848 on DRIVE and STARE respectively. It confirms that ICA affects the segmentation model because proper enhancement of vessels in the initial stage helps post-processing to generate better vessels extraction. We solved this issue by experimenting with the ICA architectures and selected the best one for retinal vessels extraction.

#### B. ANALYSIS ON THE EFFECT OF SCALE NORMALIZATION

Contrast normalization plays an important role in the vessel segmentation process. This is elaborated as the fourth stage of the proposed algorithm. Four fixed constant parameters ( $\alpha$  and  $\beta$ ) are part of the contrast normalization technique. It is very important to conduct an experiment to obtain the optimal parameters. For this reason, we have selected four cases, and their performances are recorded on the DRIVE and STARE databases. These four cases are

- 1) Case 1:  $\alpha = 0.5$  and  $\beta = 0.5$ .
- 2) Case 2:  $\alpha = 1$  and  $\beta = 0.5$ .
- 3) Case 3:  $\alpha = 1.5$  and  $\beta = 0.5$ .
- 4) Case 4:  $\alpha = 1$  and  $\beta = 0.5$ .

Fig. 16 shows the performance measure of these four cases. It is clearly observed that in both databases sensitivity, accuracy, and specificity are affected by scale normalization factors ( $\alpha, \beta$ ). The accuracy increases when  $\alpha$  value also

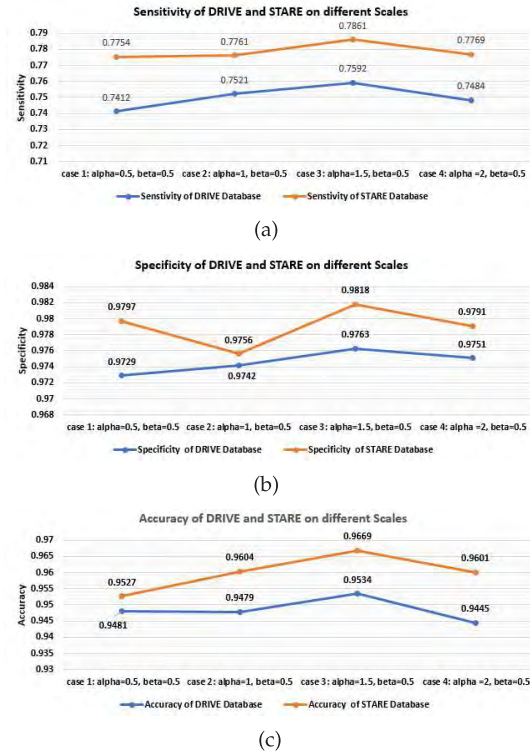


**FIGURE 16.** Observation of tiny vessels with an effect of scale normalization proposed cases. Fig. (a) shows the curve of the sensitivity of DRIVE and STARE databases, Fig. (b) shows the curve of specificity of DRIVE and STARE databases, and Fig. (c) shows the curve of the accuracy of DRIVE and STARE databases.

increases but the sensitivity decreases beyond  $\alpha = 1$ . The main theme of this research work is boosting the sensitivity of the vessels by improving the ability to detect tiny vessels. On the basis of such an experiment, case 2 gives the best performance in terms of sensitivity and accuracy. We considered the results derived from case 2 for our segmentation model.

#### C. ANALYSIS THE AFFECT OF STOPPING TIME OF ANISOTROPIC DIFFUSION FILTER

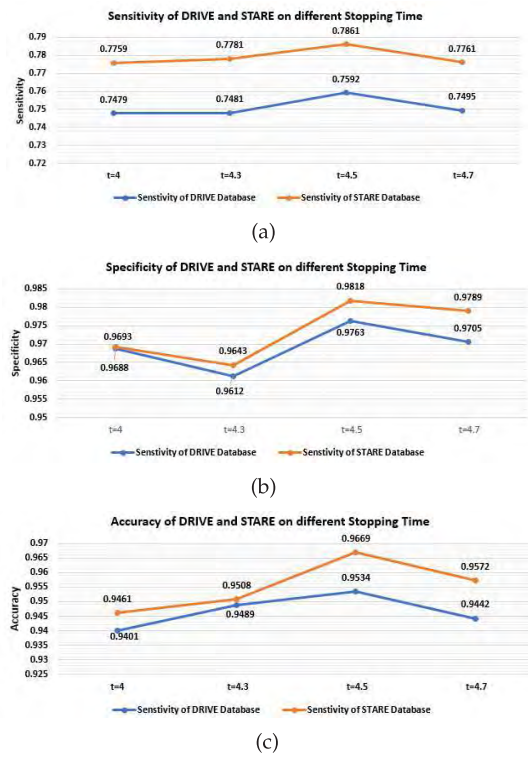
The stage 5 of our algorithm contains anisotropic diffusion that needs an appropriate diffusion time. In this particular section, the objective performance based on four different cases of stopping time: Case 1:  $t = 4$ ; Case 2:  $t = 4.3$ ; Case 3:  $t = 4.5$  and Case 4:  $t = 4.7$ . Fig. 17 shows sensitivity, specificity and accuracy data of DRIVE and STARE database for these four cases of stopping time. It is observed that both sensitivity and accuracy are increasing for case 1, 2 and 3, but they drop in the case 4. The highest sensitivity, as well as accuracy, is obtained at  $t = 4.5$ . Experimentally, the  $t = 4.5$  is adopted as optimal stopping time for proposed algorithm.

#### D. PERFORMANCE ON CHALLENGING IMAGES

We analyzed the performance of our method on noisy pathological images, and the vessels segmentation results for such images are shown in Fig. 18(d) and Fig. 18(h). The performance of the proposed method is compared with two novel methods named Nuygen [29] and Hou [30] as

**TABLE 1.** Performance analysis of segmentation model.

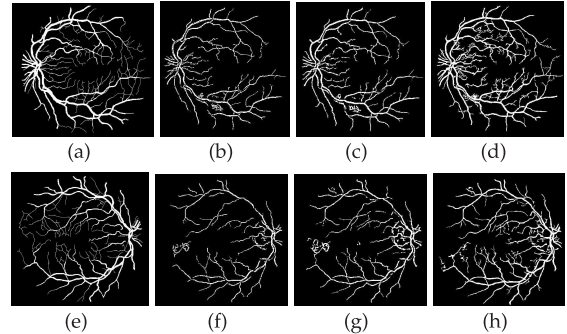
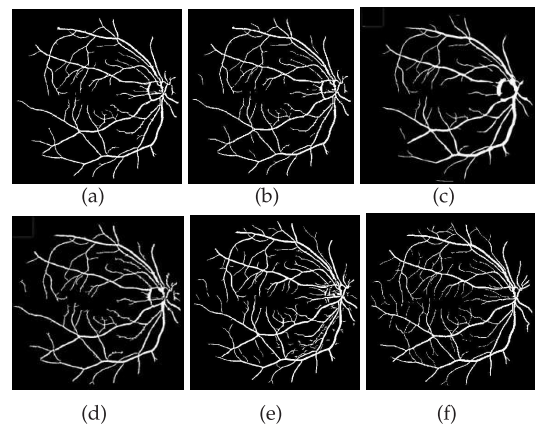
Methods	Se	DRIVE		Se	STARE	
		Sp	AC		Sp	AC
<b>Supervised Methods</b>						
Steal et al [19]	-	-	0.946	-	-	0.951
Soares et al [11]	-	-	0.946	-	-	0.948
Lupascu et al [42]	0.720	-	0.959	-	-	-
Orlando et al [41]	0.785	0.967	-	-	-	0.951
Liskowski [43]	-	-	0.949	-	-	0.949
<b>Unsupervised Methods</b>						
Mendonca et al [37]	0.734	0.976	0.945	0.699	0.973	0.944
Matinez-Perez et al [44]	0.724	0.965	0.934	0.750	0.956	0.941
Palomera-Perez et al [45]	0.66	0.961	0.922	0.779	0.940	0.924
Nguyen et al [29]	-	-	0.940	-	-	0.932
Xiaoxia Yin et al [46]	-	-	0.947	-	-	-
Zhao et al (FR Method) [40]	0.682	0.867	0.853	0.634	0.967	0.938
Zhao et al (IWT Method) [40]	0.716	0.978	0.944	0.776	0.954	0.943
Zhao et al (IPACHI Method) [40]	0.742	0.982	0.954	0.780	0.978	0.956
Soomro et al [47]	0.713	0.968	0.941	0.711	0.965	0.942
Khan et al [48]	0.734	0.967	0.951	0.736	0.971	0.95
Soomro et al [33]	0.753	0.976	0.943	0.784	0.981	0.961
<b>Proposed Method</b>	0.752	0.976	0.953	0.786	0.982	0.967

**FIGURE 17.** Stopping time analysis of anisotropic diffusion filtering on retinal images of four different stopping times. a) shows the sensitivity of DRIVE and STARE databases. b) shows the specificity of DRIVE and STARE databases. c) shows the accuracy of DRIVE and STARE databases.

shown in Fig. 18. It can be clearly observed that the methods of Hou and Nuygen drop tiny vessels when compared to our proposed method.

#### E. OBSERVATION OF TINY VESSELS

While many segmentation methods have been proposed, there are two disadvantages observed in virtually all methods: firstly, missing the tiny vessels; and secondly, the

**FIGURE 18.** Capabilities of the proposed segmentation model are tested on the challenging images. Consider Fig (a) and Fig (e) is manually segmented images. Fig (d) and Fig (h) show the output segmented images of our proposed method compared to the results of Nuygen (shown in Fig (b)) and Hou (shown in Fig (f)) and Zhao (shown in Fig (c) and Fig (g)).**FIGURE 19.** Fig (e) shows the results of our proposed segmentation method, and is comparable to the output of Nguyen et al [29] (as shown in Fig (a)), Hou [30] (as shown in Fig (b)) and Zhao et al [40] (as shown in Fig (c) and Fig (d)) along with gold standard image (as shown in Fig (h)).

sensitivity decreases. Both these limitations only can be solved by properly detecting tiny vessels which improves sensitivity. We compared the output of our method regarding

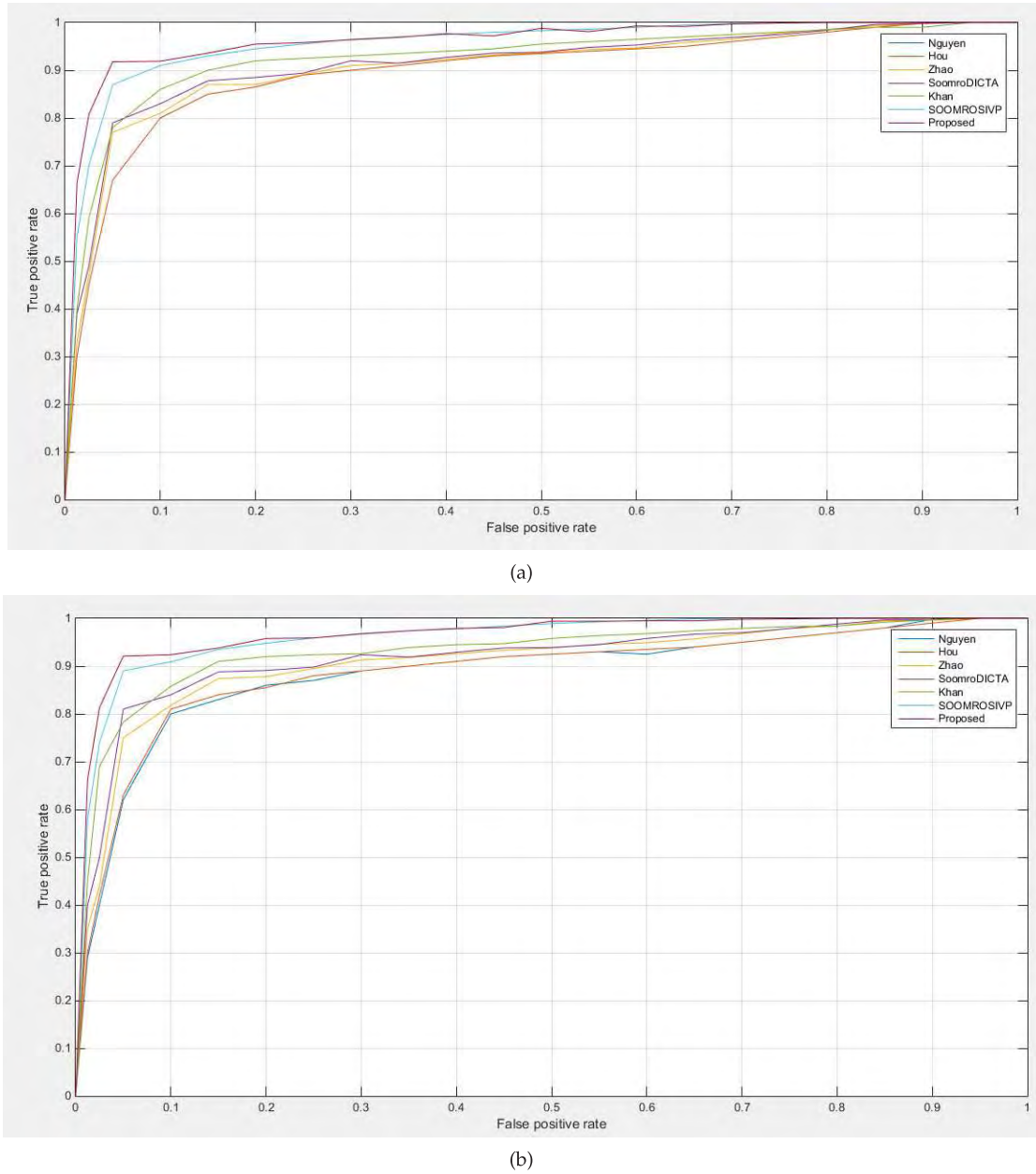


**FIGURE 20.** a) ROC curve for classification on the DRIVE database. b) ROC curve for classification on the STARE database.

the issues of tiny vessels with those applications used by Nguyen *et al* [29], Hou [30] and Zhao *et al* [40]. Fig. 19 shows the output image of Nguyen (Fig 19(a)), Hou (Fig 19(b)), Zhao FR (Fig. 19(c)) and the wavelet-based segmentation method (Fig 19(d)). It can be clearly observed that the proposed method detects more tiny vessels compared to the methods of Nguyen, Hou, and Zhao. The output of our proposed method is, in fact, comparable to the gold standard image (Fig 19(f)). It proves experimentally that our method successfully detects tiny and large vessels properly, it provides eye experts the opportunity for observing the progression of eye disease.

#### F. COMPARISON TO OTHER METHODS

To prove the capability of detection of retinal blood vessels, we compared our proposed retinal vessels segmentation methods with existing state-of-the-art methods. Two publicly available databases named DRIVE and STARE are used for evaluation purpose. Table 1 shows a comparison of the performance of our method with other existing methods. In comparison with supervised methods, our proposed gave a higher sensitivity of  $Se = 0.75$  than other supervised methods, except Orlando and Blaschko [41] method that has slightly higher sensitivity than our method. Similarly, comparison of our proposed method with unsupervised methods also

shows comparable performance with existing state-of-the-art methods.

The receiver operating characteristic curves (ROC) of our proposed method on the STARE and DRIVE databases are also computed and compared with the ROC of other methods. ROC curve gives information between false positive pixels and true positive pixels in the form of fractions according to change in threshold on the probability map. The ROC curve indicated good performance by observing the curve closer towards the left corner. We compared the ROC of our proposed method with seven methods [29], [30], [33], [40], [47], [48], [48]. We computed the ROC curve of these methods [33], [47], [48] to compare it with our proposed method. From ROC curves, it can be observed that the curve of the proposed method is increasing at the true positive rate that indicates better performance of proposed method than all other seven existing methods.

## IX. CONCLUSION

The automatic vessel imaging analysis tool has been demonstrated to be a reliable tool for accurate segmentation of retinal images. In this research effort, we have implemented and validated an image contrast enhancement technique based on ICA architecture 2 (ICA2). The aim was to address the problem of varying intra-image contrast and its adverse effect on correct image segmentation.

We have shown that combining our proposed ICA-based image enhancement technique with the segmentation model has achieved higher levels of segmentation accuracy and classification. With certain modifications, the ICA2 image enhancement procedures described in this study can be extended to other subdomains of medical imaging where the detection of low-contrast features has proven to be a non-trivial problem.

## REFERENCES

- [1] N. Patton, T. Aslam, T. MacGillivray, A. Patti, I. J. Deary, and B. Dhillon, "Retinal vascular image analysis as a potential screening tool for cerebrovascular disease: A rationale based on homology between cerebral and retinal microvasculatures," *J. Anatomy*, vol. 206, no. 4, pp. 319–348, 2005.
- [2] H. Kanaide, T. Ichiki, J. Nishimura, and K. Hirano, "Cellular mechanism of vasoconstriction induced by angiotensin II it remains to be determined," *Circulat. Res.*, vol. 93, pp. 1015–1017, Nov. 2003.
- [3] M. M. Fraza *et al.*, "Blood vessel segmentation methodologies in retinal images—A survey," *Comput. Methods Programs Biomed.*, vol. 108, no. 1, pp. 407–433, 2012.
- [4] T. A. Soomro, J. Gao, M. A. U. Khan, T. M. Khan, and M. Paul, "Role of image contrast enhancement technique for ophthalmologist as diagnostic tool for diabetic retinopathy," in *Proc. Int. Conf. Digit. Image Comput., Techn. Appl. (DICTA)*, Nov. 2016, pp. 1–8.
- [5] T. A. Soomro, J. Gao, T. M. Khan, A. F. M. Hani, M. A. U. Khan, and M. Paul, "Computerised approaches for the detection of diabetic retinopathy using retinal fundus images: A survey," *J. Pattern Anal. Appl.*, vol. 20, no. 4, pp. 927–961, 2017.
- [6] J. J. Wang *et al.*, "Retinal vessel diameter and cardiovascular mortality: Pooled data analysis from two older populations," *Eur. Heart J.*, vol. 28, no. 16, pp. 1984–1992, 2007.
- [7] P. J. Saine and M. E. Tyler, *Ophthalmic Photography: Retinal Photography, Angiography and Electronic Imaging*, 2nd ed. Boston, MA, USA: Butterworth-Heinemann, 2002.
- [8] B. Cassin and S. A. B. Solomon, *Dictionary of Eye Terminology*, 2nd ed. Gainesville, FL, USA: Triad Publishing Company, Mar. 1990.
- [9] H. M. Pakter *et al.*, "Measuring arteriolar-to-venous ratio in retinal photography of patients with hypertension: Development and application of a new semi-automated method," *Amer. J. Hypertension*, vol. 18, no. 3, pp. 417–421, 2005.
- [10] T. Y. Wong *et al.*, "Computer-assisted measurement of retinal vessel diameters in the beaver dam eye study: Methodology, correlation between eyes, and effect of refractive errors," *J. Ophthalmol.*, vol. 111, no. 6, pp. 1181–1190, 2004.
- [11] J. V. B. Soares, J. J. G. Leandro, R. M. Cesar, H. F. Jelinek, and M. J. Cree, "Retinal vessel segmentation using the 2-D Gabor wavelet and supervised classification," *IEEE Trans. Med. Imag.*, vol. 25, no. 9, pp. 1214–1222, Sep. 2006.
- [12] A. Hyvärinen, "Fast and robust fixed-point algorithms for independent component analysis," *IEEE Trans. Neural Netw.*, vol. 10, no. 3, pp. 626–634, May 1999.
- [13] A. C. Jirapatnakul, S. V. Fotin, A. P. Reeves, A. M. Biancardi, D. F. Yankelevitz, and C. I. Henschke, "Automated nodule location and size estimation using a multi-scale laplacian of gaussian filtering approach," in *Proc. 31st Annu. Int. Conf. IEEE EMBS*, vol. 1, Sep. 2009, pp. 1028–1031.
- [14] B. Zhang, L. Zhang, L. Zhang, and F. Karraya, "Retinal vessel extraction by matched filter with first-order derivative of Gaussian," *Comput. Biol. Med.*, vol. 40, no. 4, pp. 438–445, 2010.
- [15] P. Bankhead, C. N. Scholfield, J. G. McGeown, and T. M. Curtis, "Fast retinal vessel detection and measurement using wavelets and edge location refinement," *PLoS ONE*, vol. 7, no. 3, p. e32435, 2012.
- [16] G. Lathen, J. Jonasson, and M. Borga, "Blood vessel segmentation using multi-scale quadrature filtering," *Pattern Recognit. Lett.*, vol. 31, no. 8, pp. 762–767, 2010.
- [17] D. Lesage, E. D. Angelini, I. Bloch, and G. Funka-Lea, "A review of 3D vessel lumen segmentation techniques: Models, features and extraction schemes," *Med. Image Anal.*, vol. 13, no. 6, pp. 819–845, Aug. 2009.
- [18] K. Sun, Z. Chen, and S. Jiang, "Local morphology fitting active contour for automatic vascular segmentation," *IEEE Trans. Biomed. Eng.*, vol. 59, no. 2, pp. 464–473, Feb. 2012.
- [19] J. Staal, M. D. Abramoff, M. Niemeijer, M. A. Viergever, and B. V. Ginneken, "Ridge based vessel segmentation in color images of the retina," *IEEE Trans. Med. Imag.*, vol. 23, no. 4, pp. 501–509, Apr. 2004.
- [20] X. You, Q. Peng, Y. Yuan, Y.-M. Cheung, and J. Lei, "Segmentation of retinal blood vessels using the radial projection and semi-supervised approach," *Pattern Recognit.*, vol. 44, no. 10, pp. 10–11, 2011.
- [21] E. Ricci and R. Perfetti, "Retinal blood vessel segmentation using line operators and support vector classification," *IEEE Trans. Med. Imag.*, vol. 26, no. 10, pp. 1357–1365, Oct. 2007.
- [22] C. Sinthanayothin, J. F. Boyce, H. L. Cook, and T. H. Williamson, "Automated localisation of the optic disc, fovea, and retinal blood vessels from digital colour fundus images," *Brit. J. Ophthalmol.*, vol. 83, no. 8, pp. 890–902, 1999.
- [23] D. Marin, A. Aquino, M. E. Gegúndez-Arias, and J. M. Bravo, "A new supervised method for blood vessel segmentation in retinal images by using gray-level and moment invariants-based features," *IEEE Trans. Med. Imag.*, vol. 30, no. 1, pp. 146–158, Jan. 2011.
- [24] B. Al-Diri, A. Hunter, and D. Steel, "An active contour model for segmenting and measuring retinal vessels," *IEEE Trans. Med. Imag.*, vol. 28, no. 9, pp. 1488–1497, Sep. 2009.
- [25] F. Rossant, M. Badellino, A. Chavillon, I. Bloch, and M. Paques, "A morphological approach for vessel segmentation in eye fundus images, with quantitative evaluation," *J. Med. Imag. Health Informat.*, vol. 1, no. 1, pp. 42–49, 2011.
- [26] Y. Matsuda and K. Yamaguchi, *Gram-Schmidt Orthonormalization to the Adaptive ICA Function for Fixing the Permutation Ambiguity*. Cham, Switzerland: Springer, 2016, pp. 152–159.
- [27] R. W. Knighton, "Quantitative reflectometry of the ocular fundus," *IEEE Eng. Med. Biol. Mag.*, vol. 14, no. 1, pp. 43–51, Jan. 2002.
- [28] T. T. J. M. Berendschot, P. J. DeLintb, and D. van Norren, "Fundus reflectance—Historical and present ideas," *Progr. Retinal Eye Res.*, vol. 2, no. 22, pp. 171–200, 2003.
- [29] U. T. V. Nguyen, A. Bhuiyan, L. A. F. Park, and K. Ramamohanarao, "An effective retinal blood vessel segmentation method using multi-scale line detection," *Pattern Recognit.*, vol. 46, no. 3, pp. 703–715, 2013.
- [30] Y. Hou, "Automatic segmentation of retinal blood vessels based on improved multiscale line detection," *J. Comput. Sci. Eng.*, vol. 8, no. 2, pp. 119–128, 2014.

- [31] M. A. U. Khan, T. M. Khan, T. A. Soomro, N. Mir, and J. Gao, "Boosting sensitivity of a retinal vessel segmentation algorithm," *Pattern Anal. Appl.*, pp. 1–17, Oct. 2017, doi: <https://doi.org/10.1007/s10044-017-0661-4>
- [32] *Studio Encoding Parameters of Digital Television for Standard 4:3 and Wide Screen 16:9 Aspect Ratios*, document ITU-R BT.601-5, 1995.
- [33] T. A. Soomro, M. A. U. Khan, J. Gao, T. M. Khan, and M. Paul, "Contrast normalization steps for increased sensitivity of a retinal image segmentation method," *J. Signal Image Video Process.*, vol. 11, no. 8, pp. 1509–1517, 2017.
- [34] C. Gottschlich and C.-B. Schonlieb, "Oriented diffusion filtering for enhancing low-quality fingerprint images," *IET Biometrics*, vol. 1, no. 2, pp. 105–113, Jun. 2012.
- [35] T. Lindeberg, "Feature detection with automatic scale selection," *Int. J. Comput. Vis.*, vol. 30, no. 2, pp. 79–116, 1998.
- [36] J. Fehrenbach and J.-M. Mirebeau, "Sparse non-negative stencils for anisotropic diffusion," *J. Math. Imag. Vis.*, vol. 49, no. 1, pp. 123–147, 2014.
- [37] A. M. Mendonca and A. Campilho, "Segmentation of retinal blood vessels by combining the detection of centerlines and morphological reconstruction," *IEEE Trans. Med. Imag.*, vol. 25, no. 9, pp. 1200–1213, Sep. 2006.
- [38] R. C. Gonzalez and R. E. Woods, *Digital Image Processing*, 3rd ed. Englewood Cliffs, NJ, USA: Prentice-Hall, 2006.
- [39] A. D. Hoover, V. Kouznetsova, and M. Goldbaum, "Locating blood vessels in retinal images by piecewise threshold probing of a matched filter response," *IEEE Trans. Med. Imag.*, vol. 19, no. 3, pp. 203–210, Mar. 2000.
- [40] Y. Zhao, L. Rada, K. Chen, S. P. Harding, and Y. Zheng, "Automated vessel segmentation using infinite perimeter active contour model with hybrid region information with application to retinal images," *IEEE Trans. Med. Imag.*, vol. 34, no. 9, pp. 1797–1807, Sep. 2015.
- [41] J. I. Orlandi and M. Blaschko, "Learning fully-connected crfs for blood vessel segmentation in retinal images," in *Proc. Med. Image Comput. Comput. Assist. Intervent. (MICCAI)*, vol. 17. 2014, pp. 634–641.
- [42] C. A. Lupas, D. Tegolo, and E. Trucco, "FABC: Retinal vessel segmentation using adaboost," *IEEE Trans. Inf. Technol. Biomed.*, vol. 14, no. 5, pp. 1267–1274, Sep. 2010.
- [43] P. Liskowski and K. Krawiec, "Segmenting retinal blood vessels with deep neural networks," *IEEE Trans. Med. Imag.*, vol. 35, no. 11, pp. 2369–2380, Nov. 2016.
- [44] M. E. Martinez-Perez, A. D. Hughes, S. A. Thom, A. A. Bharath, and K. H. Parker, "Segmentation of blood vessels from red-free and fluorescein retinal images," *J. Med. Image Anal.*, vol. 11, no. 1, pp. 47–61, 2007.
- [45] M. A. Palomera-Pérez, M. E. Martinez-Perez, H. Benítez-Pérez, and J. L. Ortega-Arjona, "Parallel multiscale feature extraction and region growing: Application in retinal blood vessel detection," *IEEE Trans. Inf. Technol. Biomed.*, vol. 14, no. 2, pp. 500–506, Mar. 2010.
- [46] X. Yin, B. W.-H. Ng, J. He, Y. Zhang, and D. Abbott, "Accurate image analysis of the retina using Hessian matrix and binarisation of thresholded entropy with application of texture mapping," *PLOS ONE*, vol. 9, no. 4, pp. 1–17, 2014.
- [47] T. A. Soomro, M. A. U. Khan, J. Gao, T. M. Khan, M. Paul, and N. Mir, "Automatic retinal vessel extraction algorithm," in *Proc. Int. Conf. Digit. Image Comput., Techn. Appl. (DICTA)*, Nov. 2016, pp. 1–8.
- [48] M. A. U. Khan, T. A. Soomro, T. M. Khan, D. G. Bailey, J. Gao, and N. Mir, "Automatic retinal vessel extraction algorithm based on contrast-sensitive schemes," in *Proc. Int. Conf. Image Vis. Comput. New Zealand (IVCNZ)*, Nov. 2016, pp. 1–5.



**TOUFIQUE AHMED SOOMRO** received the B.E. degree in electronic engineering from the Mehran University of Engineering and Technology, Pakistan, in 2008, and the M.Sc. degree in electrical and electronic engineering from University Technologi PETRONAS, Malaysia, in 2014. He is currently pursuing the Ph.D. degree with the School of Computing and Mathematics, Charles Sturt University, Australia. His research interests include most aspects of image enhancement and image analysis for medical images. He is currently implementing software-based algorithm for the detection of eye-related disease.



**TARIQ MAHMOOD KHAN** received the B.S. degree in computer engineering from the COMSATS Institute of Information Technology, the M.Sc. degree in computer engineering from the University of Engineering and Technology, Taxila, Pakistan, and the Ph.D. degree from Macquarie University Sydney, NSW, Australia, in 2016. He is currently serving as an Assistant Professor with the Electrical Engineering Department, COMSATS Institute of Information Technology, Islamabad, Pakistan. He is interested in both digital image processing (with an emphasis on biometrics) and VLSI. His research interests include most aspects of image enhancement, pattern recognition, and image analysis. One area of interest is the application of FPGAs to biometric processing algorithms.



**MOHAMMAD A.U. KHAN** received the B.S. degree from UET Peshawar, Pakistan, in 1992, the M.Sc. degree from Loughborough University of Technology, U.K., in 1994, and the Ph.D. degree from Georgia Tech in 1999. Since 1999, he has been actively involved in image processing, pattern recognition, and machine learning. He published extensively in residual vector quantization, directional filterbank, retinal vessel extraction, and signature verification.



**JUNBIN GAO** received the B.Sc. degree in computational mathematics from the Huazhong University of Science and Technology (HUST), China, in 1982, and the Ph.D. degree from the Dalian University of Technology, China, in 1991. He was a Professor in computer science with the School of Computing and Mathematics, Charles Sturt University, Australia. From 1982 to 2001, he was an Associate Lecturer, a Lecturer, an Associate Professor, and a Professor with the Department of Mathematics, HUST. He was a Senior Lecturer and a Lecturer in computer science with the University of New England, Australia, from 2001 to 2005. He is currently a Professor of big data analytics with The University of Sydney Business School, The University of Sydney. His main research interests include machine learning, data analytics, Bayesian learning and inference, and image analysis.



**MANORANJAN PAUL** received the Ph.D. degree from Monash University, Australia, in 2005. He was a Post-Doctoral Research Fellow with the University of New South Wales, Monash University, and Nanyang Technological University. He is currently an Associate Professor and the Head of E-Health Research, Charles Sturt University (CSU). He received over \$15 million competitive grant money, including the most prestigious Australian Research Council Discovery Project Grant and Cybersecurity CRC. He has published over 150 refereed publications. His major research interests are in the field of data science such as data compression, video technology, computer vision, e-Health, and medical imaging/signal processing. He is the ICT Researcher of the Year 2017 awarded by the Australian Computer Society. He received the Research Excellence Supervision and Research Excellence Awards at CSU. He is the General Chair of PSIVT 2019, the Program Chair of DICTA 2018, the Program Chair of PSIVT 2017, and the Publicity Chair of DICTA 2016. He was an Invited Keynote Speaker in DICTA 2013 and 2017, CWCN 2017, WoWMoM 2014, and ICCIT 2010. He is currently an Associate Editor of the IEEE TRANSACTIONS ON CIRCUITS AND SYSTEMS FOR VIDEO TECHNOLOGY and EURASIP *Journal on Advances in Signal Processing*.



**LIHONG ZHENG** received the Ph.D. degree in computing sciences from the University of Technology, Sydney, in 2008. She is currently a Senior Lecturer with the School of Computing and Mathematics, Charles Sturt University. Her previous research interest was on automation, robotics, and artificial intelligence. She has authored and co-authored over 40 papers in the field of artificial intelligence, image processing, machine learning, and robotic, and holds one patent. Her current research interest is on computer vision, image processing, pattern recognition, and machine learning.

• • •